J. Applied Membrane Science & Technology, Vol. 9, No. 1, June 2025, 111-140

Copra Biochar Pyrolysis Optimization for Cr(VI) Removal and Membrane Incorporation Potential

A. A. A. A. Ramli[a], H. Hasbullah[a]*, J. Hamdan[a], M. N. F. M. Ghazali[a], A. N. Masri[a] & T. D. Kusworo[b]

[a]Faculty of Chemical and Energy Engineering, Universiti Teknologi Malaysia, 81310 UTM Johor Bahru, Johor, Malaysia
[b]Department of Chemical Engineering, Faculty of Engineering, Diponegoro University, Semarang 50275, Indonesia

Submitted: 28/2/2025. Revised edition: 25/3/2025. Accepted: 26/3/2025. Available online: 27/3/2025

ABSTRACT

Pyrolyzed coconut copra biochar (PCB) is a primary byproduct produced during the pyrolysis process of coconut copra biomass. This study focused on the effect of increasing pyrolysis temperature on the characteristics and hexavalent chromium (Cr(VI)) removal potential of the PCB as adsorbent and membrane precursor. Copra, a readily available agricultural waste in Malaysia, was utilized as the biochar precursor to produce PCB at 300-500 °C, 5 °C/min heating rate and 1 hour residence time. Then, PCB was incorporated into a polyvinylidene fluoride (PVDF) membrane using the dry/wet phase inversion technique, with varied biochar loadings (0 to 1 wt.%). The produced PCB were characterized using CHNS elemental analysis, Fourier transform Infrared (FTIR) spectroscopy, scanning electron microscopy (SEM), Brunaue-Emmett-Teller (BET) surface analysis and pH drift analysis to assess morphology, functional groups, surface area, porosity and pH point of zero charge, respectively. Adsorption isotherm study shows the best fit with Langmuir and Freundlich model. Adsorption kinetics study shows pseudo-second order model fit better than the pseudo-first-order model. Then, preliminary incorporation tests of optimized PCB in PVDF membrane analyzed using water uptake and porosity analysis, water contact angle and performance analysis via cross flow system to assess water flux and Cr(VI) removal. It was found at 450 °C pyrolysis temperature produced copra biochar with relatively high carbon content of 72 %, the highest pore volume of 6.168×10^{-3} cm^3/g with adsorption capacity of 10.41 mg/g and Cr(VI) removal of 27.98 %. As PCB loading in the PVDF membranes increased from 0 to 0.4 wt.%, it was found that the membrane porosity increased from 7 % to 62 % resulted in the enhancement of the water flux achieving maximum 2.04 $Lm^{-2}h^{-1}$ at 0.5 g/L loading and Cr(VI) removal achieving 33.33 %. This has shown good potential of copra biochar as adsorbent and incorporation to develop adsorptive membrane for heavy metal removal.

Keywords: Biochar, hexavalent chromium, adsorption, pyrolysis, biomass

1.0 INTRODUCTION

Clean water supply is in high demand due to the rapid growth of industries and development. Pollutants generated by industries such as metallurgy, tanneries, pharmaceuticals, and organochemicals have severely constrained clean water

* Corresponding to: H. Hasbullah (email: hasrinah@utm.my)
DOI: https://doi.org/10.11113/jamst.v29n1.312

resources [1]. Heavy metals are one of the most common contaminants in water, either naturally or from manmade causes. Human activities, particularly industrial operations, have risen considerably over the years, resulting in extensive contamination of air, water, and soil. Heavy metal discharge from industries and urban areas into the environment without sufficient treatment has become a problem due to their hazardous nature.

A guideline for heavy metals has been established by the World Health Organization, with acceptable limits of 0.05 mg/L for Chromium (Cr) and if the amounts are above the allowable limit and they are not biodegradable, they may be a concern to human health and the aquatic environment [2]. Cr can be released into the environment by both anthropogenic and natural processes. Natural sources of Cr include volcanic eruptions and weathering of rocks, but many of the pollution exists in water and soil due to numerous human activities such as chrome ore mining, metal cleaning, and plating industries [3].

Cr species, including Cr(III) and Cr(VI), remain prevalent in most habitats, but Cr(VI) is far more toxic and carcinogenic to living organisms than Cr(III), thus it is critical to reduce the environmental threats posed by Cr(VI) to human health and living organisms [4]. Numerous methods are being used to remove Cr(VI), including photocatalytic reduction, adsorption, precipitation, and biological methods. Adsorption, due to its simplicity and cost-effectiveness, has been widely used in Cr(VI) removal [5–7].

Biochar has become increasingly popular in wastewater treatment procedures due to its chemical stability, low cost, high carbon content, porosity, and surface area, as well as its being green or its environmental friendliness [1, 8–10]. The high functionality associated with biochar surface imparts adsorption potential for toxic substances present in wastewater [21]. Meanwhile, researchers from all over the world have been fascinated by the pyrolysis of carbonaceous materials, specifically biomass, into value-added products in the form of chemicals, bio-oil, gaseous products, and biochar.

Abundant biomass feedstocks such as sewage sludge and agricultural residues have been widely used to produce biochar materials. Thus, it is vital to continuously evaluate new feedstock, such as coconut wastes, for biochar production. Coconut or its scientific name as *Cocos nucifera L.* is the most consumed fruit in Malaysia and one of the most important agricultural commodities in Malaysia after palm oil, rubber and paddy. It is the oldest industrial crop in Malaysia which contributed RM 72.8 million, equivalent to 0.06 % of Malaysia's agricultural export revenue in 2020 [11, 12].

Coconut production in Malaysia increases year after year due to high demand for coconut products such as coconut milk and coconut oil. The glut of output has resulted in an excess of coconut waste, including coconut shell, coconut husk, and coconut copra waste (CCW). CCW is a by-product after coconut milk or coconut oil was extracted from the grated coconut flesh. One of the alternatives and more sustainable ways to reduce and utilize CCW is by conversion into biochar via pyrolysis process. To date, limited relevant studies have been performed on the optimization of pyrolysis temperature on coconut copra biochar with relation for Cr(VI) removal. The mechanisms involved in Cr(VI) adsorption by biochar materials are complicated, and their contributions vary depending on the type of biochar used and the reaction conditions. The adsorption mechanism of Cr(VI) with coconut copra biochar still needs thorough investigation. Recent findings of relations of pyrolyzed biochar and Cr(VI) removal are tabulated at Table 1.

Table 1 Recent research of Cr(VI) adsorption removal

Biochar/ Biosorbent	**Findings**	**Research Gap**	**Ref**
Pigeon pea leaves and chickpea stems (magnetic biochar)	Cr(VI) removal facilitated by surface complexation, reduction, and electrostatic attraction.	Limited to pigeon pea leaves and chickpea stems as biochar.	[43]
Rice Husk (amide modification)	Maximum removal efficiency 97 % at pH 2, contact time of 60 min, dosage of 2 g/L and concentration of 100 mg/L.	Incomplete characterization hinders understanding of material properties and Cr removal. BET and pHpzc analyses needed.	[44]
Corn Stalk	Maximum removal efficiency 28.67 % achieved at pH 4, biochar dosage 4.5 g/L, contact time 270 min, Cr(VI) initial concentration 60 g/L).	Low removal efficiency and limited to pH study. Lacking characterization (surface area, pores, functional groups, composition).	[45]
Rice Husk	Adsorption capacity improved due to surface area improvement after pyrolysis.	No pyrolysis optimization. No surface charges and functional groups characterization.	[46]
Onopordom Heteracanthom	SEM and BET analysis explains surface area relation. Initial concentration and pH relation in Cr(VI) solution.	Low 5.73 m^2/g adsorption capacity. Lack surface charge analysis.	[47]
Algal-derived	Maximum removal percentage of Cr (VI) is 97.88% for the metal concentration of 1 ppm.	Fixed 500 °C pyrolysis. No optimization of pyrolysis temperature.	[48]

Table 1 Recent research of Cr(VI) adsorption removal (continued)

Biochar/ Biosorbent	Findings	Research Gap	Reference
Coconut Coir	Optimization of pyrolysis temperature. Biochar pyrolyzed at 400 °C with 24 h contact time achieved 90 % Cr(VI) removal.	Limited to coconut coir biochar. Lack surface characterization crucial in understanding biochar ability of Cr(VI) removal.	[49]
Coconut Fiber-Polyaniline Composites	Best adsorptions happen at pH4 in 30 minutes with 0.25 mg/ml dosage	Limited to Coconut Fiber	[50]
Coconut Copra	Removal of Cd, Cr and Ni with average 96 %, Optimized dosage 0.1 g and pH 8.48	Copra not pyrolyzed into biochar and optimization were a combination of Cd, Cr and Ni.	[51]

Derived via pyrolysis, biochar is a cost-effective and environmentally conscious alternative to activated carbon in membrane applications [13]. Studies indicate that copra biochar's high carbon content and pore formation capabilities lead to excellent surface area, making it a viable option for modifying membrane structures [14]. Thus, copra biochar in this study need focus on its pore formation and surface area which relates to the main pyrolysis process parameters which is pyrolysis temperature variation. Then, the integration of biochar potentially improves the surface and structure properties of polymeric membranes to achieve high permeation flux, suitable for wastewater treatment [14, 15].

Biochar is generally more environmentally friendly and cost-effective than activated carbon [13] Researchers have also explored porous biochar derived from aerobic granular sludge for high-performance membrane [16]. PVDF (polyvinylidene fluoride) is a common material due to its excellent chemical resistance, thermal stability, mechanical strength and functionalization approaches to develop PVDF membrane nanocomposites for environmental applications [17]. Studies have explored incorporating biochar into PVDF membranes to enhance their performance for the separation of organic matter from water [18].

Thus, the main goals of this study were to (1) compare and optimize pyrolysis temperature in production of Pyrolyzed Copra Biochar (PCB); (2) evaluate Cr(VI) adsorption performance on PCB under variations of conditions and (3) investigate the effect of PCB loadings in PVDF/PVP membrane on the filtration of Cr(VI). Therefore, this research aimed to investigate the efficacy of PCB utilized for Cr(VI) removal from synthetic wastewater. The physicochemical characteristics of PCB were studied by employing CHNS Elemental Analysis, FTIR, SEM, BET surface area and point of zero charge analyses.

2.0 METHODS

2.1 Materials

CCW obtained by the white coconut flesh dregs waste after the coconut milk had been extracted in domestic household and stalls uses in Skudai, Johor. CCW was collected and washed thoroughly under running tap water to remove dirt and foreign matters. It was then oven-dried at 105 ºC and weighed repeatedly until constant weigh was achieved then kept in airtight container. Potassium Dichromate, $K_2Cr_2O_7$, ACS reagent, ≥ 99.0 % by Sigma Aldrich was used to prepare stock of synthetic Cr(VI) solution which further diluted for uses by distilled water in particular concentrations. NaOH and HNO_3 also from Sigma Alrich were diluted to 0.1M solutions to adjust the pH of Cr(VI) solutions in adsorption tests. The filtrates of adsorption tests were subjected to atomic absorption spectrometer (AAS) using Micromeritics TriStar II 3020 Version 3.02.

2.2 Preparation of Varied Pyrolyzed Copra Biochar (PCB)

Coconut copra biomass that had been grounded and sieved was used to make biochar by pyrolysis in a tubular reactor with a heating rate of about 20°C min^{-1} and a nitrogen flow of 0.4 L min^{-1}, pyrolysis was carried out at six different temperatures produced PCB at 300 °C, 350 °C, 400 °C, 450 °C, 500 °C and 550 °C. (PCB300, PCB350, PCB400, PCB450, PCB500 and PCB550) The highest reaction temperature was held constant for 1 hour to guarantee that the reactions were completed. Yield (%) calculations are as follows.

$$Y_{BC} = \frac{Product_{BC}}{Feed_{Bm}} \times 100 \qquad (1)$$

$$Y_{BO} = \frac{Product_{BO}}{Feed_{Bm}} \times 100 \qquad (2)$$

where Y_{BC} and Y_{BO} are the yield of biochar and bio-oil in percentage (%) respectively, whereas $Product_{BC}$ and $Product_{BO}$ are the weight of products which is biochar and bio-oil collected after pyrolysis respectively while $Feed_{Bm}$ is the weight of biomass feed before pyrolysis in gram (g).

2.2.1 Characterization of PCB

PCB samples gone through several characterization and analysis. CHNS Elemental Analysis determine the composition of each PCB samples. Although XRD analysis would provide insights into the amorphous carbon structure and the degree of graphitization, particularly from the (100) and (002) peaks, XRD analysis was not performed as this study focus on the changes of biochar surface area, pore sizes and functional groups due to the pyrolysis temperature variations.

Therefore, FTIR spectroscopy was executed to classify the changes of various compounds associated with biochar as the pyrolysis temperature of varied. KBr powder was mixed with biochar to produce pellets. SEM were executed to study the surface properties present on the surface of PCB powder which is placed on a metal stub and undergoes silver sputtering before observed in 1.5k magnification. In addition, BET Analysis executed to determine BET surface area and pore volume. The point of zero charge (pH_{pzc}) of PCB biochar samples was determined using the pH drift method. In this method, 0.1 g/L of biochar was added to 100 mL of 0.1 M potassium nitrate KNO_3 solution. The initial pH was adjusted from 2 to 11 using 0.1 M HNO_3 or 0.1 M KOH stirred for 24 hours at 30 °C, and the final pH was measured. The pH_{pzc} was identified as

the x-intercept of a plot of the difference between the initial and final pH against the initial pH

2.2.2 Adsorption Tests of PCB for Cr(VI) Removal

The batch adsorption was performed for treatment of synthetic hexavalent chromium, Cr(VI) solution with PCB samples (0.1 g/L) as adsorbents. 100 mL of 5 mg/L Cr solution was added to a 100 mL flask, and pH was maintained at 2.0 without adjustment. Parameters were based on optimized variables from prior research to focus on adsorption analysis of PCB samples pyrolyzed at different temperatures. Preparation of stock solution of Cr(VI), cleaning of flasks, and dilution of stock solution to obtain desired concentration of Cr(VI) solution was done by using distilled water to maintain purities. The mix of biochar and solution stirred for 24 hours (to ensure equilibrium) at a temperature of 30 °C. The removal rate (%) of Cr(VI) and adsorption capacity is obtained by employing the following equations:

$$R = \frac{C_o - C_e}{C_o} \times 100 \quad (3)$$

$$q_e = \frac{(C_o - C_e) \times V}{M} \quad (4)$$

where R is the removal rate in percentage (%) while Co and Ce are initial and equilibrium concentration of Cr(VI) in mg/L. q_e is adsorption capacity of adsorbent in mg/g. V is volume of Cr(VI) solution in litre (L), and M represents adsorbent dose mass in gram (g). Atomic Absorption Spectrometer (AAS) executed for the filtrate of batch adsorption tests in determining Cr(VI) removal of PCB samples and optimizing the pyrolysis temperature for copra generation as biochar adsorbent as Cr(VI) removal application.

Following PCB450 optimization, further batch adsorption tests were conducted to optimize adsorption parameters independently. The parameters investigated included pH (2-11, adjusted with 0.1 M HNO_3 and 0.1 M KOH), initial Cr concentration (1-200 mg/L), contact time (1-1440 min), and PCB dosage (0.1-1.5 g/L), while maintaining consistent stirring and filtration procedures and consequently replaced the optimized parameters. The removal rate (%) of Cr(VI) and adsorption capacity obtained by employing the same equations of Eq. 3 and Eq. 4 through the Atomic Absorption Spectrometer (AAS) Analysis. Adsorption Isotherm and Kinetics study also calculated to observe the Adsoprtion Isotherm and Kinetic model fitting.

2.3 Loading of Optimized PCB Sample into PVDF Membrane

Preliminary study of incorporating optimized PCB samples into membrane were carried out to test PCB ability as membrane filler. Polyvinylidene Fluoride/ Polyvinylpyrrolidone (PVDF/PVP) flat sheet membranes were fabricated via dry/wet phase inversion. 3 wt.% PVP was dissolved in 80 wt.% NMP at 70 °C with continuous stirring. Optimized PCB samples were then added at varied concentrations (0.0-5.0 wt.%) and mixed until homogenous. Finally, 17 wt.% dried PVDF was added and stirred at 350 rpm for 24 h to ensure complete dissolution and prevent biochar agglomeration. A 0.06 mm thick film was cast from a dope solution onto a glass plate using a glass rod and feeler blade. After 10 seconds of air exposure, the film was immersed in a distilled water bath for precipitation. Once detached, the membrane was soaked in water for 3 days (with regular water changes) followed by an 8-hour methanol bath to

remove residual PVP and solvent. The membrane was then air-dried at room temperature for 24 hours and stored in a sealed container.

Pure PVDF with PVP but without PCB (M0) also fabricated following the same procedure for control measure and observation purposes. M0, MPCB1, MPCB2, MPCB3, MPCB4 and MPCB5 prepared according to loading of optimized PCB at 0, 0.1, 0.2, 0.3, 0.4, 0.5 and 1.0 wt.% respectively.

2.3.1 Characterization of PCB Incorporated PVDF/PVP Membrane

The membrane immersed in water for 48 hr to reach saturation of water in the membrane. After removing the excess water on the surface with tissue paper, the weight of the wet membrane measured. Then, the membrane dried at 50 °C in the oven and the weight of the dried membrane measured. Eq.5 and Eq. 6 used to calculate the water uptake, ω and overall porosity, φ respectively.

$$\omega = \frac{W' - W}{W'} \times 100 \quad (5)$$

$$\varphi = \frac{W' - W}{\rho \times V} \times 100 \quad (6)$$

where, W' is wet membrane weight (g), W is dried membrane weight (g), ρ is pure water density at 25 °C (1 g cm^{-3}) and V is the dried membrane effective volume (cm^3). The membranes' water contact angles (°) observed using an Optical Contact Angle analyser. The membrane piece placed in horizontal position with the membrane's targeted surface facing up. Distilled water drop injected from a micro-syringe with a stainless-steel needle onto the target membrane surface. The instrument captured and analysed the instant drop image on the membrane surface to determine the water CA value.

2.3.2 Water Flux and Cr(VI) Filtration Performance Analysis through Crossflow System

A crossflow filtration system with 1 L/min feed flow rate used to test the effect of cross flow rate. First, the membrane compacted at 1.5 bar in pure water for 30 minutes to ensure that it achieves steady-flux conditions. The feed water pumped across the membrane's surface layer from one end of the module to the other, and the permeate withdrawn from the membrane. Distilled water and Cr(VI) solution are independently used as the feed solution. AAS used to determine Cr(VI) concentration in the permeate and feed samples (as initial concentration comparison). The filtration experiment then be carried out at pressure of 2 bar gauge and the membrane pure water flux (J_{W1}) calculated using Eq.7 where, V is volume of permeate (L), A is membrane effective area (m2) and t is filtration time to collect the permeate.

$$J_{w1} = \frac{V}{A\Delta t} \times 100 \quad (7)$$

$$\varphi = \frac{W' - W}{\rho \times V} \times 100 \quad (8)$$

3.0 RESULTS AND DISCUSSION

3.1 Effect of Varied Pyrolysis Temperature on PCB Samples Characteristics

3.1.1 Yield and CHNS Elemental Analysis

Generally, higher temperatures are preferred for biomass pyrolysis as a higher temperature induces the pyrolysis process to run completely and fulfill the decomposition and carbonization process especially if bio-oil focused and further proved increase the bio-oil yield as shown in Figure 1. However, the biochar yield decreases as pyrolysis temperature increases. The carbonization process was probably completed when pyrolysis temperature was at 500 °C as the biochar yield shows a constant average value of 11% [16]. Although lower temperature seems to guarantee higher production of biochar yield, CHNS Elemental Analysis further shows a significantly lower carbon content recorded in the lower pyrolysis temperature in comparison to the higher pyrolysis temperature as shown in Figure 2 signifying higher carbon produced at higher pyrolysis temperature. C content increased whereas H and O content decreased by rising pyrolysis temperature as shown in Figure 2

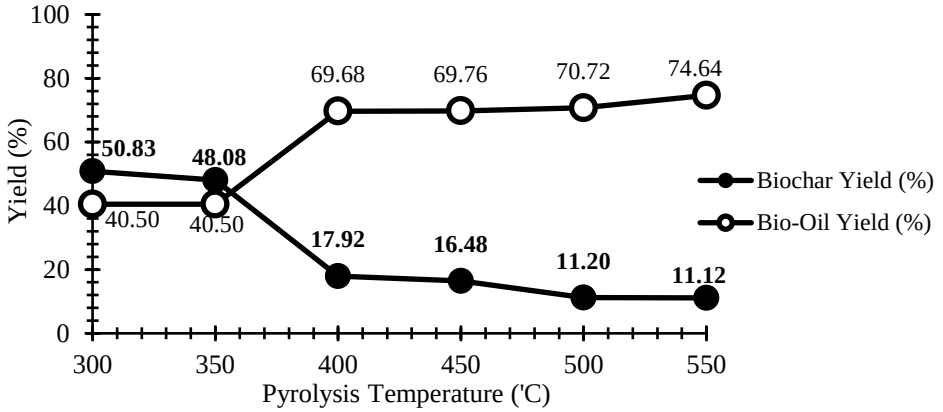

Figure 1 Biochar and Bio-oil collected at varied Pyrolysis Temperature (°C)

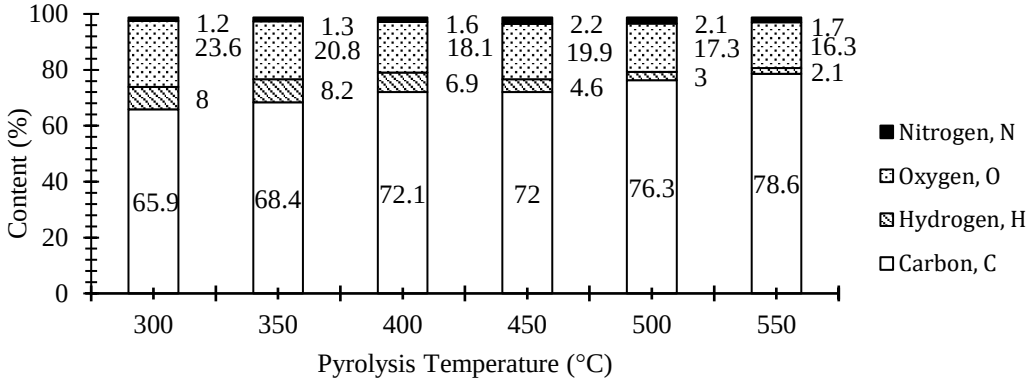

Figure 2 Carbon, Hydrogen, Oxygen and Nitrogen Content (%) against Pyrolysis Temperature (°C)

Based on Figure 3, the comparison of biochar yield and its carbon content clearly shows a diverging trend of significant increase of carbon content as the pyrolysis temperature increases despite the declining copra biochar yield. Therefore, higher pyrolysis temperature produces better quality of copra biochar with higher carbon content percentage that is crucial in improving its Cr(VI) adsorption capacity in Adsorptions Tests. H/C is a common metric for assessing the degree of carbonization. Based on Figure 3, H/C reduction indicated that the degree of carbonization of copra biochar had risen. O/C can reflect the degree of aromatization, and the polarity of biochar produced. Based on Figure 4, O/C ratio seems to be decreasing too implying the drop of the content of oxygen-containing functional groups which are hydroxyl and carboxylic acid abundances [17, 18]. Therefore, higher pyrolysis temperature resulted in an increase in carbon density of the biochar and increased the rate of dehydration and volatilization which encouraged oxygen removal. Fourier Transform Infrared Spectroscopy (FTIR) needed to prove and concur the decreasing functional groups forecasted by the H/C and O/C ratio.

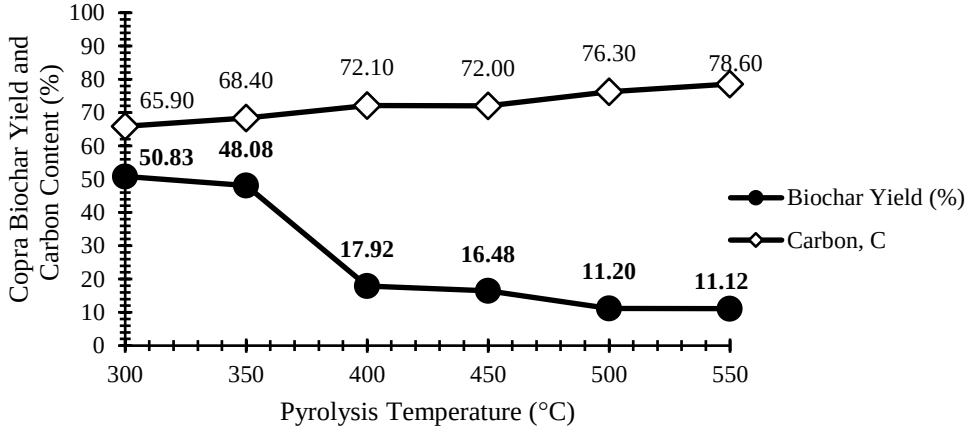

Figure 3 Copra Biochar Yield and Carbon Content (%) against Pyrolysis Temperature (°C)

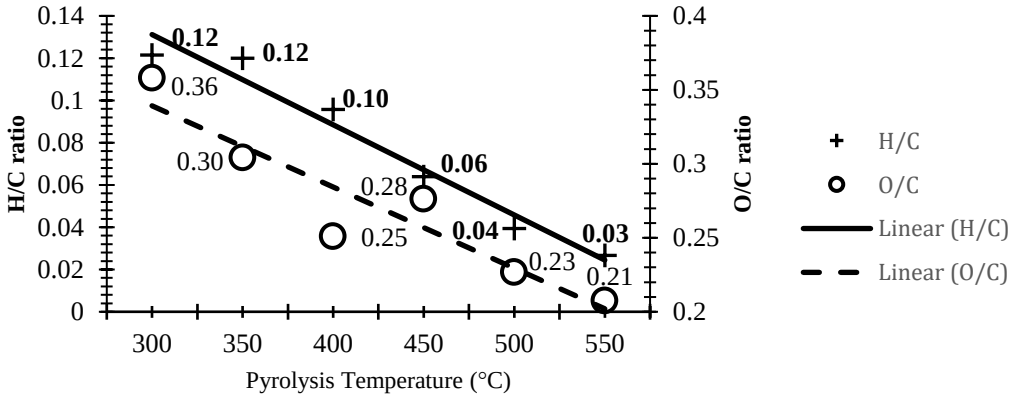

Figure 4 H/C and O/C ratio against Pyrolysis Temperature (°C)

3.1.2 Fourier Transform Infrared Spectroscopy (FTIR)

Functional groups of PCB Samples are determined through FTIR Analysis to see the effect of pyrolysis temperature towards functional group and bonding presence. The presence of biochar surface functional groups through FTIR transmittance analysis with varied pyrolysis temperature were illustrated in Figure 5. The presence of H groups (polar), C-H groups (polar), C-C groups, C-O groups (polar), C=C groups, C=O and C=H were determined by the peaks in Figure 5.

As pyrolysis temperature increases, these functional groups decrease and diminish as shown in Figure 5., which further concurred the loss of hydrogen and oxygen bonded groups and the decline of H/C and O/C ratio determined before. This is because at higher pyrolysis temperatures, the degree of carbonization accelerates and intensifies, leading to the rapid loss of volatile compounds. The biochar samples' FTIR spectra display a broad peak at 3394 cm^{-1} indicatives of the hydroxyl groups in alcohol and phenolic hydroxyl groups of O–H bonds stretching [19].

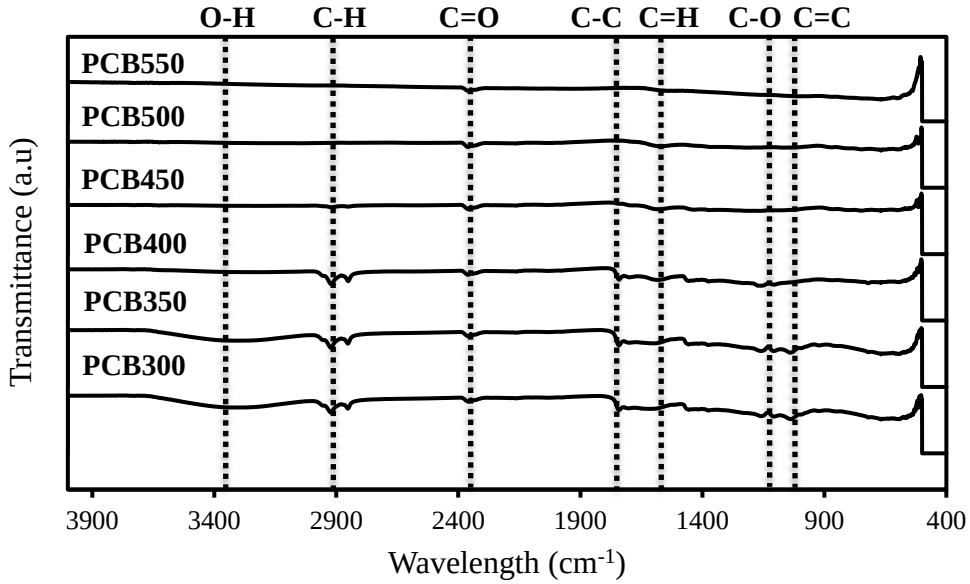

Figure 5 FTIR of PCB Samples

The intensity of the O-H bonds stretching broad peak was found to be stronger at lower temperatures (PCB300 and PCB350) while the broad peak slopes decreased and become more even out at higher temperatures (as shown from PCB400 towards PCB550). At 2927 cm^{-1}, FTIR displays the distinctive C–H stretching vibration of the aliphatic group's alkyl structure. The stretching of carbonyl bonds (C=O) in carboxylic groups or conjugated ketone is represented by the peak at 1693 cm^{-1}. At 1597 cm^{-1}, the aliphatic –C=C– stretching vibrations are apparent. As functional groups decrease, the specific surface area of copra biochar will increase as too high abundance of oxygen-containing functional groups will occupy a certain space and clog some pores, diminish the pore volume, and cause the collapse of the pore wall furthermore decrease the specific surface area [20]. Thus, increasing pyrolysis temperature reduce functional groups which indicates the increase of biochar surface area and pore volume formation.

3.1.3 Scanning Electron Microscopy (SEM)

Based on Figure 6, the pore size concurred to be affected by the increasing pyrolysis temperature in conjunction of the results of rising functional groups in FTIR Analysis. Based on Figure 6 (a) to (f), SEM images show that more pores form on the copra biochar as the temperature of pyrolysis increases. Figure 6 (a), (b) and (c) shows underdeveloped, blocked pores and collapsing pore walls due to higher abundance of functional groups which concurred with the results of FTIR Analysis.

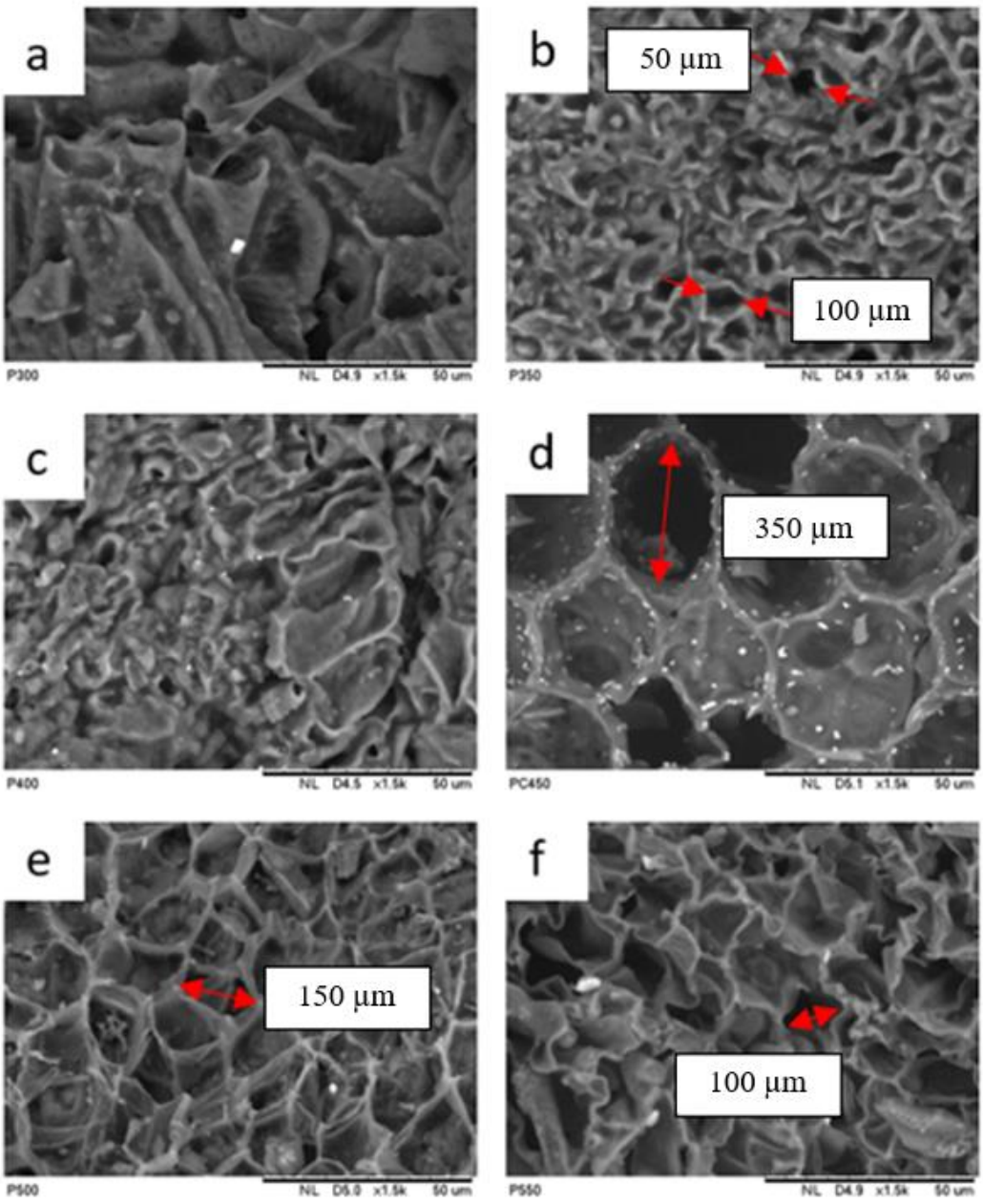

Figure 6 SEM images of (a) PCB300 (b)PCB350 (c)PCB400 (d)PCB450, (e)PCB500, (f)PCB550 at magnification x1.5k

The size of pore formed also increases as the pyrolysis temperature increases while the pore sizes range decrease in value. Best instance shown for the image of PCB450 with pore sizes range (400-450) µm. Based on Figure 6 (d), PCB450 structures shown with fully developed uniform pores with largest diameter which generated at 450 °C. Then, Figure 6 (e) and (f) show that the pores formed at 500 °C and 550 °C were irregularly generated and show signs of ruptures especially in Figure 6 (f). The least value of pore size range also exhibits in PCB450 with least difference value of all PCB samples which is 25 µm which means an evenly size pores generated as clearly shown in Figure 6 (d). Therefore, the optimum temperature range of achieving fully developed uniformed pores happens at pyrolysis temperature range 450 °C.

3.1.4 Brunauer Emmett Teller (BET) Analysis

Based on Table 2, PCB450 and PCB500, pore volumes are 6.168x10-3 cm^3/g and 6.728x10-3 cm^3/g, respectively. PCB450 (450 °C) shows a high pore volume with a 1.865 m2/g surface area. PCB500 (500 °C) also has a high pore volume, but a significantly lower surface area of 0.1821 m^2/g. This suggests similar pore formation at both temperatures, but pore wall deformities at 500 °C cause a drastic drop in surface area, in contrast to the steady increase seen from 300 °C to 450 °C. Lower surface areas at 300 and 350 °C are likely to be due to underdeveloped pores and clogging by volatile compounds. Higher pyrolysis temperature often increases the surface area and carbonized fraction of biochar, leading to a high sorption capability for pollutants. The pore size and distribution of a given biochar can affect its utility and controlling the high pyrolysis temperature is the most common way to affect this [20]. These results complementing the previous SEM images of biochar pore formation fully formed at 450 °C and pore walls structure collapsed at 500 °C and 550 °C. The total pore volume also drops significantly to $2.78x10^{-3}$ cm^3/g concurring the results of PCB550 SEM image of ruptured pores. Intense heat in higher pyrolysis temperatures (500 °C and 550 °C) cause pore walls to melt and restructured post the completed carbonization process leading to a decrease in the overall pore volume and surface area of the biochar [21, 22].

Table 2 BET Surface Area (m^2/g) and Total Pore Volume $x10^{-3}$ (cm^3/g) of PCB samples at variation of Pyrolysis Temperature (°C)

Copra Biochar	Pyrolysis Temperature (°C)	BET Surface Area (m^2/g)	Total Pore Volume $x10^{-3}$ (cm^3/g)
PCB300	300	0.042	2.512
PCB350	350	0.525	3.692
PCB400	400	1.041	5.721
PCB450	450	1.865	6.168
PCB500	500	0.182	6.728
PCB550	550	0.087	2.780

PCB450 BET surface area, 1.865 m²/g is a relatively low compared to many other common adsorbents like activated carbon, zeolites, or some metal-organic frameworks (500 to 1500 m^2/g). However, biochar surface areas varied

If the adsorption mechanism relies more on chemical interactions (chemisorption) rather than physical adsorption (physisorption), achieving too high of values of surface area might not be as critical optimization [26].

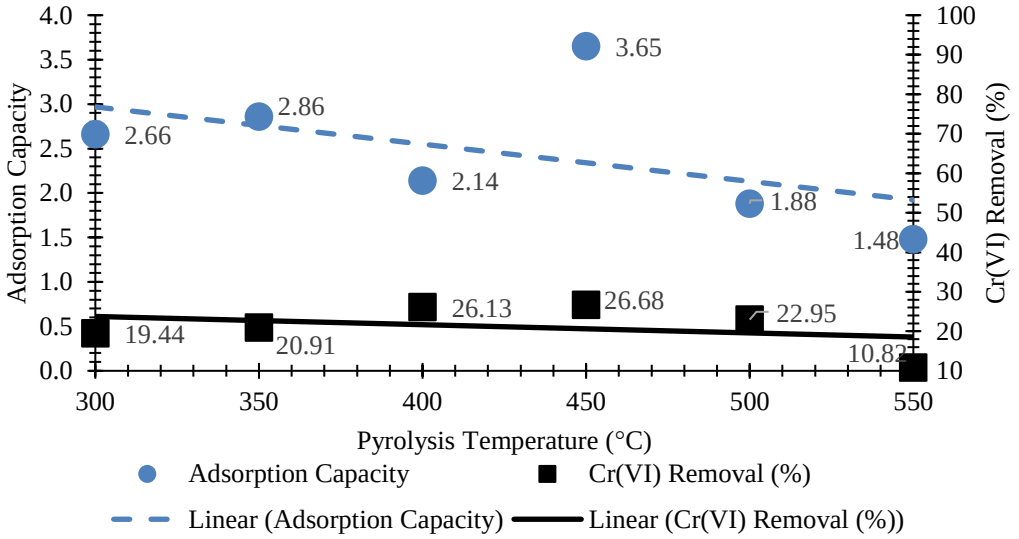

Figure 7 PCB Adsorption Capacity, q_e (mg/g) and Cr(VI) Removal (%) against Pyrolysis Temperature (°C)

A based on the type of feedstock and conditions in pyrolysis process and mostly acquired very low surface areas (below 10 m²/g), while others can be much higher (hundreds of m²/g). Although PCB450 has a maximum achieved surface area of 1.865 m²/g which is on the lower end, it doesn't automatically disqualify it from being an effective adsorbent [23]. The presence of functional groups and surface chemistry of the material does support the relevancy of PCB450 as Cr(VI) adsorbent. Even with a low surface area, if the biochar has enough specific functional groups (e.g., amine groups, carboxyl groups) that have a high affinity for Cr(VI), it can still be effective which shown in previous FTIR analysis [24]. Besides, biochar can facilitate the reduction of Cr(VI) to less toxic and less mobile Cr species. This redox activity can be more influential than a high surface area [25]. direct comparison with other materials tested under similar conditions would provide a clearer picture of its effectiveness.

3.2 Batch Adsorption Tests of PCB Samples with Cr(VI) Solution

3.2.1 Cr(VI) Adsorption Tests of PCB Samples with Preliminary Parameters

Generally, higher pyrolysis temperature will increase the adsorption capacity thus improving Cr(VI) removal performance [27]. Based on Figure 7, Cr(VI) adsorption increased from 300 °C to 450 °C, but decreased after 500 °C. With a constant initial concentration of 1 mg/L, pH 4.4, and 0.1 g/L biochar dosage, PCB450 achieved the highest Cr(VI) removal (26.68%), with removal decreasing at pyrolysis temperatures of 500 °C and 550 °C. The removal

mechanism of Cr(VI) from solution was regarded as an adsorption-coupled reduction [28]. The biochar produced have increased microporous structures and functional groups, and consequently, exhibited an improved adsorption capacity for Cr(VI) [29].

All the parameters are preliminary referenced by combination of previous research as shown in Table 1. The contact time was left for 24 hours to ensure maximum equilibrium adsorption. Adsorption capacity also shows similar trend of results with the highest adsorption capacity recorded for PCB450 (3.65 mg/g). Therefore, 450 °C chosen and proven as the optimized pyrolysis temperature which shows the best performance results complementing the characterizations results of high carbon density in CHNS Elemental Analysis, the highest pore volume and highest surface area in BET Analysis.

The pH_{pzc} of PCB450 also shows PCB450 biochar form have suitable surface charges for Cr(VI) ion species to be attracted to the surfaces of biochar pores without hindering characteristics due to the high basicity and repulsive charges on the surfaces of PCB500 and PCB550 thus explaining the declining results of adsorption capacity and Cr(VI) removal for PCB500 and PCB550.

3.2.2 Optimization of Cr(VI) Solution pH

The parameter of pH of the solution has significant importance during the sorpyio sorption process. The variation in pH affects the process of diffusion, charges at the surface, and linking properties of metal and metalloid ions after speciation. The charge on the biochar surface can be maintained by changing the pH. As the charge on biochar surface modifies, metal and metalloid ions' specification will also vary. Thus, variation in pH has critical impacts on Cr(VI) adsorption and removal.

Table 3 PCB450 Adsorption Capacity, q_e (mg/g) and Cr(VI) Removal (%) with variations of pH

pH	Adsorption Capacity, q_e (mg/g)	Cr(VI) Removal (%)
2	99.96	38.52
3	27.05	10.42
4	18.52	7.13
4.4	19.40	7.48
6	29.64	11.42
8.48	36.02	13.88
11	14.631	5.64

Given the importance of pH, the adsorption was carried out by changing the pH within the range of 2 to 11 using PCB450. At the lower pH (acidic) of 2, highest 99.96 mg/g chromium was adsorption recorded then dropped significantly after pH 3 as shown in Table 3. As pH increased from 3 to 8.48, the adsorption of Cr(VI) slightly increases approaching neutral pH range and at pH 11, 14.63 mg/g Cr(VI) was adsorbed showing declining adsorption capacity and removal in high pH (basic). This proves that the adsorption

was highest at an acidic pH and lower at a basic pH.

The highest sorption value observed was at pH 2. At an acidic pH, the biochar sorbent surfaces were positively charged, while Cr(VI) exist as negatively charged chromate ions in aqueous solution, thus pH 2 was selected as the best pH for Cr(VI) adsorption process with PCB450. At pH 11, however, the hydroxyl ions' concentration was increased due to excess OH- ions and the surface of the biochar and chromium ions in the solution repelled each other due to repulsive forces.

3.2.3 Optimization of Adsorption Contact Time

Table 4 illustrates how increasing contact time benefits Cr(VI) adsorption by biochar, up to a point. The initial rapid adsorption phase, where a substantial amount of Cr(VI) is removed within 60 minutes, can be attributed to the abundance of available binding sites on the biochar surface [30]. As contact time extends, more Cr(VI) ions could diffuse into the biochar's pore structure and interact with these sites, leading to further adsorption [31]. The eventual plateau in adsorption, observed after approximately two hours (120 minutes), suggests that the available binding sites become saturated. Several mechanisms can contribute to Cr(VI) removal by biochar, including electrostatic attraction, surface complexation and physical adsorption within the pores [32]. The available surface area on the biochar plays a role as contact time increases. As more sites become occupied, fewer are available for incoming Cr(VI) ions. At this stage, competition between Cr(VI) ions for the limited remaining sites becomes a significant factor, hindering further adsorption [33].

Table 4 PCB450 Adsorption Capacity, q_e (mg/g) and Cr(VI) Removal (%) with variations of Contact Time (minutes)

Contact Time (min)	Adsorption Capacity, q_e (mg/g)	Cr(VI) Removal (%)
1	0.38	3.78
5	0.66	6.55
10	0.70	7.01
30	1.22	12.19
60	2.49	24.94
120	3.84	38.39
480	3.86	38.55
1440	3.85	38.52

3.2.4 Optimization of Cr(VI) Solution Initial Concentration

Different concentrations of Cr(VI) were added at optimized pH 2 with a contact time of 2 h. Cr(VI) concentration values variation were 1, 5, 25, 50, 100, 150 and 200 mg/L and there is a direct relation between the initial concentration and removal (%). At low concentration, a higher Cr(VI) removal recorded. As the initial concentration increased from 1 to 200 mg/L, the gradual increase in adsorption capacity was observed. At

the concentration of 100 mg/L, about 130.12 mg/g Cr(VI) adsorption was obtained, but after that the adsorption capacity became almost constant. At 200 mg/L, the Cr(VI) removal was very limited to only 6.56 %. The reason for this decline could be that large amounts of negatively charged ions did not interact with the surface of the biosorbent due to disturbances in the binding forces. The divergence of relation of adsorption capacity and Cr(VI) removal was because adsorption capacity is a normalized value, whereas removal percentage is a relative measure dependent on the initial concentration. Then, Cr(VI) removal in % is more susceptible in optimizing the best performance of PCB450 due to initial concentration variation. The decline Cr(VI) removal (%) of PCB450 with increasing Cr(VI) concentration may be due to a fixed biochar dosage thus increased competition for available binding sites relative to the increase of Cr(VI) concentration in solutions [34].

Table 5 PCB450 Adsorption Capacity, q_e (mg/g) and Cr(VI) Removal (%) against Initial Cr(VI) concentration (mg/L)

Initial Concentration (mg/L)	Adsorption Capacity, q_e (mg/g)	Cr(VI) Removal (%)
1	3.65	26.68
5	10.41	27.98
25	63.01	24.28
50	127.50	25.50
100	130.12	13.01
150	132.67	8.84
200	131.23	6.56

3.2.5 Optimization of PCB450 Dosage

This study investigates the chromium removal efficiencies of PCB450. The dosage parameter is important because it influences the uptake of Cr(VI) from the solution. Table 6 shows that increasing the biochar dosage from 0.22 g/L to 1.0 g/L resulted in average removal values of approximately 30 %. 0.8 g/L shows the highest removal value of 33.19 %, likely due to the increased availability of exchangeable sites. Further increasing the dosage to 1.0 g/L did not significantly improve Cr(VI) adsorption, remaining around 30 %. This limited improvement may be attributed to overlapping and overcrowding of biosorbent particles at the sorption sites, slightly reducing Cr(VI) adsorption at the highest dosage. The decline in adsorption with increasing biochar dose could be due to the saturation of biochar adsorption active sites, and an increased diffusion pathway caused by the aggregation of biochar particles reducing surface area [35].

Table 6 PCB450 Adsorption Capacity, q_e (mg/g) and Cr(VI) Removal (%) against dosage (g/L)

Biochar Dosage (g/L)	Adsorption Capacity, q_e (mg/g)	Cr(VI) Removal (%)
0.1	4.21	30.77
0.2	4.31	31.51
0.4	4.09	29.90
0.8	4.54	33.19
1.0	3.80	27.78

As the values showing small significant differences, 0.1 g/L was enough to be considered as optimized value of PCB450 dosage to avoid biochar aggregation using higher biochar dosage.

3.2.6 Adsorption Isotherm and Kinetics

The isotherm equations were fitted to Freundlich and Langmuir models as illustrated in Figure 8 and 9. It was observed that the Freundlich model reported the 1/n value during the Cr(VI) adsorption on PCB as <1, indicates a less favourable adsorption process, with the adsorption intensity increasing as the concentration increases. However, the R_2 value obtained in the Langmuir model was higher (0.979) compared to R_2 calculated in the Freundlich model (0.477). The outcomes of the isotherm modeling suggested that Cr(VI) adsorption was due to monolayer adsorption, which was controlled by the chemisorption process.

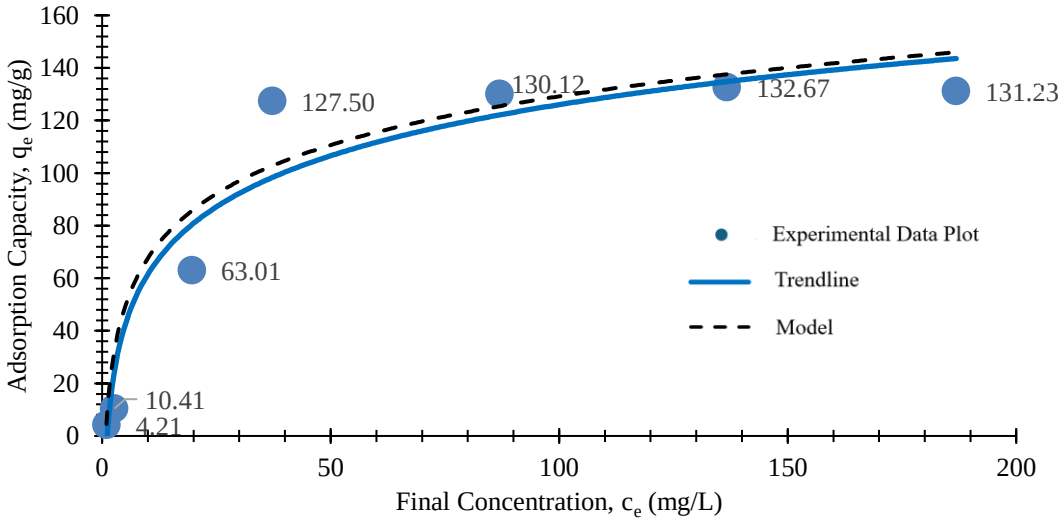

Figure 8 Adsorption Capacity, q_e (mg/g) against Final Concentration, c_e (mg/L) in comparison with Langmuir Isotherm Model

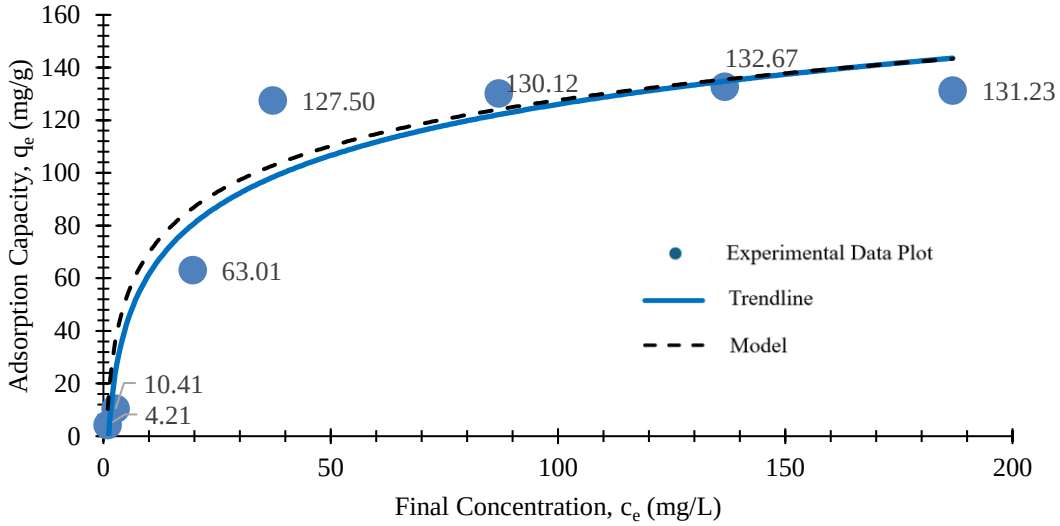

Figure 9 Adsorption Capacity, q_e (mg/g) against Final Concentration, c_e (mg/L) in comparison with Freundlich Isotherm Model

The adsorption of Cr(VI) onto PCB450 was investigated using pseudo-first-order (PFO) and pseudo-second-order kinetic (PSO) models to determine the adsorption rate (Figures 10 and 11). The model results, presented in Table 8, indicate that the PSO model (R2 = 0.998) provided a significantly better fit for the experimental data compared to the PFO model (R2 = 0.518). Furthermore, the q_e value calculated from the PSO model (3.949 mg/g) was substantially higher than that from the PFO model (0.999 mg/g). These findings suggest that the availability of adsorption sites on PCB450 influences the Cr adsorption rate, and that chemisorption is the primary mechanism, as evidenced by the superior fit of the PSO model.

Table 7 Isotherm model values for Cr(VI) adsorption on the PCB450

Isotherm Model	Parameters	Values
Langmuir	Q_L	156.462
	R_2	0.979
	K_L	0.037
Freundlich	Q_F	19.937
	R_2	0.477
	n	72.993
	1/n	0.014

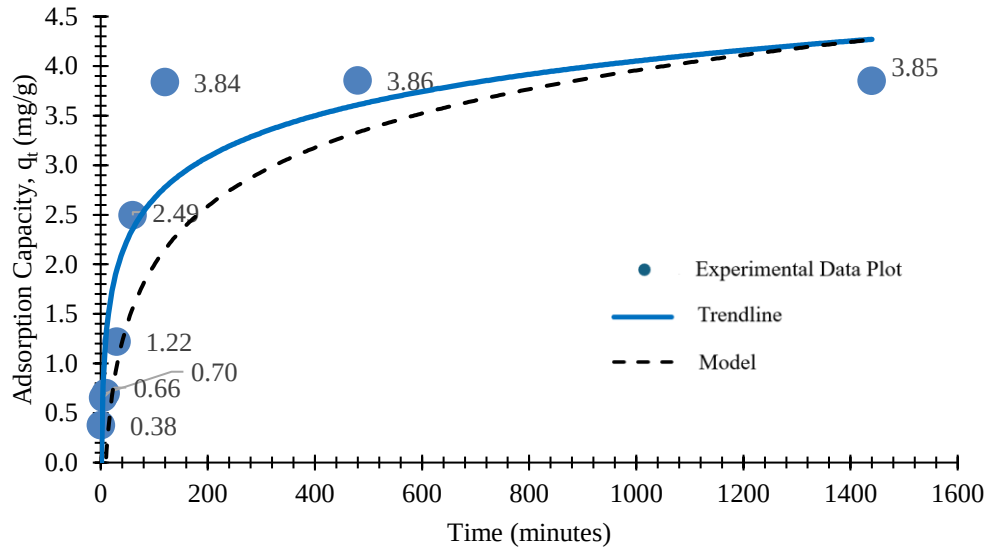

Figure 10 Adsorption Capacity, q_t (mg/g) against Contact Time (minutes) in comparison with Pseudo First Order Model

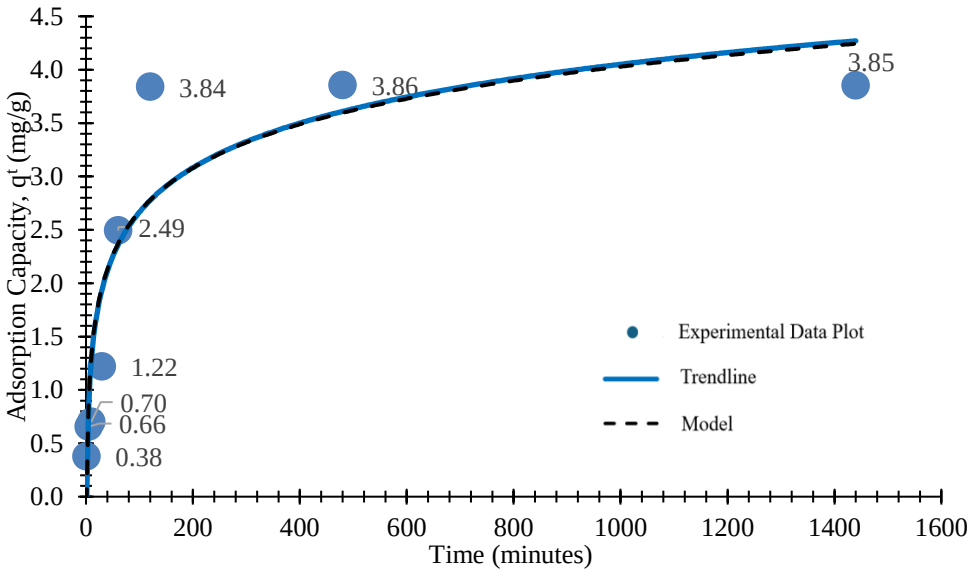

Figure 11 Adsorption Capacity, q_t (mg/g) against Contact Time (minutes) in comparison with Pseudo Second Order Model

3.2.7 Revaluation Adsorption Tests of PCB Samples with Optimized Parameters

Based on previous optimization, revaluation of Cr(VI) adsorption of PCB samples carried out with optimized parameters which was 0.1 g/L of biochar dosage with 5 mg/L or 5 ppm initial concentration of Cr(VI) solution at pH 2 in 2 h of contact time at 30 °C. Based on Figure 12, the performance results trendline shown improvement of values than the preliminary adsorption. The plotting of average Atomic Absorption Spectrometer (AAS) results shows increasing PCB samples adsorption capacity and Cr(VI) removal in the filtrate from 300 °C to 450 °C but starts to drop after 500 °C. The highest Cr(VI) removal achieved for PCB450 (27.98 %) and decreases gradually shown by PCB pyrolyzed at 500 °C and 550 °C. Adsorption capacity also shows same trend of results with the highest adsorption capacity recorded for PCB450 (10.41 mg/g) Therefore, 450 °C concurred the preliminary adsorption test of the optimized pyrolysis temperature for copra biochar which showing with improvement of results values relatively especially PCB450 (highest 27.98 % Cr(VI) removal and 10.41 mg/g adsorption capacity). This further proved that PCB450 observed with the best performance results complementing the characterizations results of high carbon density in CHNS Elemental Analysis, the highest pore volume and highest surface area in BET Analysis. The pH_{pzc} of PCB450 also shows PCB450 biochar form have suitable surface charges for Cr(VI) ion species to be attracted to the surfaces of biochar pores without hindering characteristics due to the high basicity and repulsive charges on the surfaces of PCB500 and PCB550 thus explaining the declining results of adsorption capacity and Cr(VI) removal for PCB500 and PCB550. The comparison of PCB450 Cr(VI) removal performance with other published biochar results are tabulated in Table 9.

Table 8 Kinetic model values for Cr(VI) adsorption on the PCB450

Kinetic Model	Parameters	Values
PFO	q_e (mg/g)	0.999
	$k_1(min^{-1})$	0.01
	R_2	0.518
PSO	q_e (mg/g)	3.949
	$K_2(g\ mg^{-1}min^{-1})$	0.009
	R_2	0.998

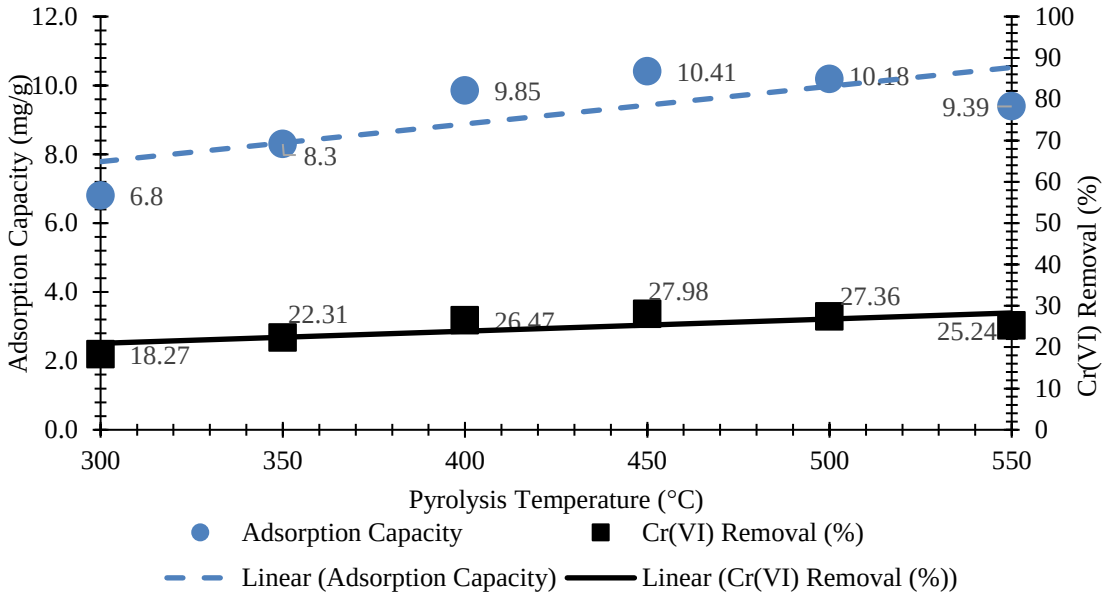

Figure 12 PCB Adsorption Capacity, q_e (mg/g) and Cr(VI) Removal (%) against Pyrolysis Temperature (°C)

Table 9 Adsorption capacity of PCB450 and comparison with other biochars

Biochar	Cr(VI) Removal (%)	Reference
Coconut Copra	27.98	This Study
Corn Stalk	28.67	[45]
Algal derived	97.8	[48]
Coconut Coir	90	[49]
Coconut Fiber	93.11	[50]

3.3 Preliminary Study of PCB450 Loading in PVDF Membrane

3.3.1 Water Uptake and Porosity Analysis of PCB450 Incorporated Membrane

Generally, higher membrane hydrophilicity is preferred for optimum water permeation, especially since biochar is favored to be more hydrophobic for optimum Cr(VI) adsorption. Based on Figure 13, water uptake of membrane samples increased from 20 % to 60 % as PCB450 loading increased from 0 wt.% to 0.4 wt.%. This demonstrates that copra biochar loadings in PVDF adsorptive membranes promote greater space for water flow. Membrane water uptake also correlates with membrane porosity, which increased from 7 % to 62 % as PCB450 loading increased from 0 wt.% to 0.4 wt.%. Higher membrane hydrophilicity is desirable for optimal water permeation, even when biochar, as a precursor, is more hydrophobic to enhance Cr(VI) adsorption. The increased PCB loading in MPCB samples leads to greater water uptake and porosity. This increased porosity provides more space for water to flow through the membrane, while the more hydrophobic copra biochar enhances contact with Cr(VI) anions, preventing water blockage at adsorption sites. Based on Figure 13, the water uptake and porosity results start to drop and further PCB450 loading of 1.0 wt.% observed a much significant drop which marks as saturation limit of PCB450 loading. Thus, all the consequent characterization and testing were limited to 0.5 wt.% because the membrane starts to be saturated and dense above 0.5 wt.% loading.

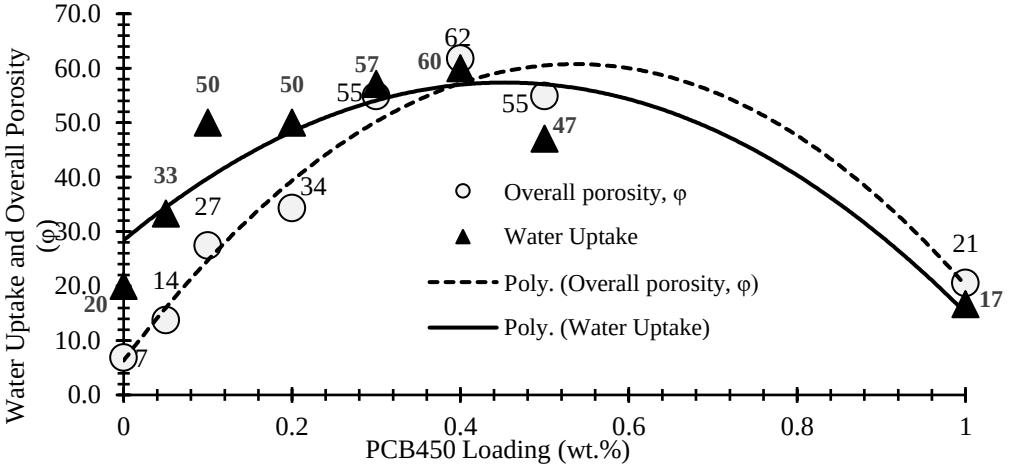

Figure 13 Water Uptake and Overall Porosity (φ) PCB450 loading (wt.%)

3.3.2 Water Contact Angle

Based on the observation in Figure 14, the water contact angle increases following the increases of PCB450 loading. In circumstances where water exhibits slight affinity to the solid surface, low contact angles (usually below 90°) are attained as shown for PCB450 loading (0.1-0.5) wt.% in Figure 14. The contact angle trendline decreases as PCB450 loading increases with the lowest contact angle value 77.73 ° at 0.5 wt.%. The balance between biochar hydrophobicity for Cr(VI) adsorption and overall membrane hydrophilicity for water permeation appears to be a key factor in optimizing membrane performance [36, 37]. It also aligns with the findings that the highest

water permeability is expected to be obtained at moderate hydrophilicity, neither at the extreme hydrophilicity nor at the extreme hydrophobicity is a good membrane for water permeation and pollutant removal [36]. The creation of surface hydrogen bonds and the dominance of adhesion forces over repulsive ones serve as the mechanism for this interaction to happen [38]. Thus, water or solutions were allowed to pass through the porous structure of the membrane easier and moisten bigger surface areas thanks to the stabilization of the forces.

This further explains and concurred the water uptake and porosity analysis [38].

As said previously, lower contact angles (typically below 90°) indicate a greater affinity of water for the solid surface [39]. In this context, the decreasing contact angle suggests that the modified membranes are becoming more hydrophilic with increased PCB450 loading, which aligns with the earlier observation of increased water uptake and porosity [38]. Therefore, membrane samples hydrophilicity improved as the PCB450 loading increases, suggesting improvement in the later adsorptive permeation membrane tests with higher affinity at PCB450 loading 0.5 wt.%.

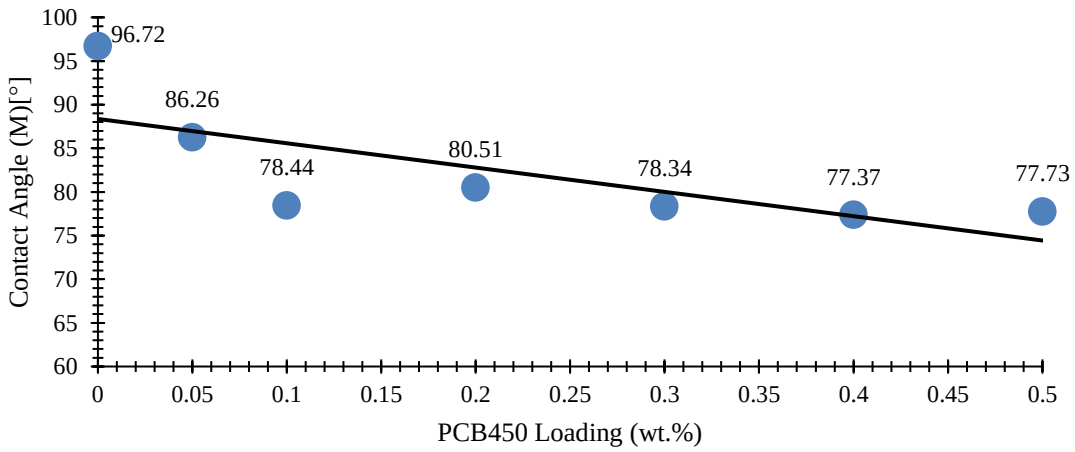

Figure 14 Water Contact Angle against PCB450 loading (wt.%)

3.3.3 Water Flux

In water flux performance tests using a Cross Flow Filtration System, higher water flux indicates improved hydrophilicity of the polymeric membrane. This is supported by characterization results showing increased water uptake and porosity, along with SEM images revealing high surface area structures. Higher hydrophilicity allows water or solutions to flow more easily through the membrane, facilitating contact with active sites for pollutant separation. In contrast, strong hydrophobicity repels water, hindering proper flow and optimal adsorption. Figure 15 shows that the pure water flux significantly increased with PCB loading (wt.%), peaking at 0.5 wt.%.

A lower flux was recorded at loadings below 0.4 wt.%, ranging from 0.48 to 1.11 $Lm^{-2}h^{-1}$, while higher values of 1.92 $Lm^{-2}h^{-1}$ and 2.04 $Lm^{-2}h^{-1}$ were observed for PCB loadings of 0.4 wt.% and 0.5 wt.%, respectively. Therefore, 0.5 wt.% is the optimized biochar loading in a PVDF/PVP adsorptive membrane, projecting higher affinity for Cr(VI) adsorption removal.

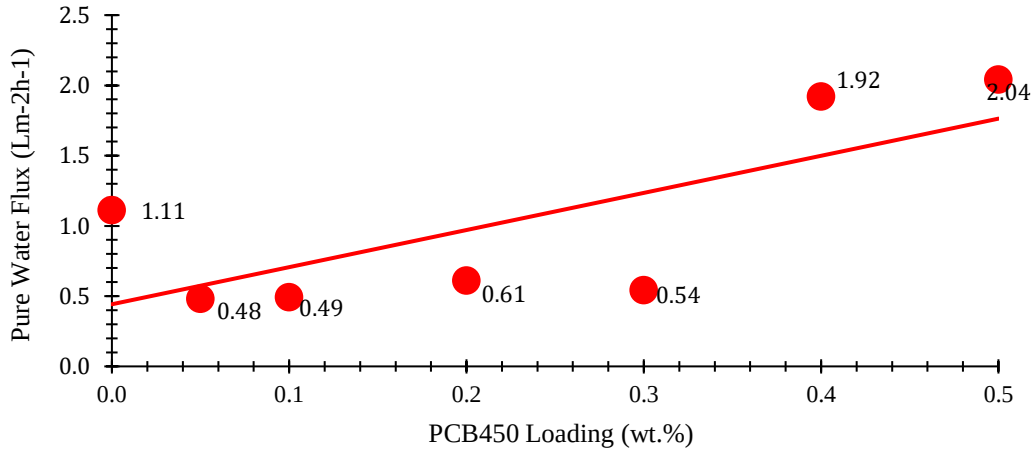

Figure 15 Pure Water Flux ($Lm^{-2}h^{-1}$) against Weight Percentage of PCB450 Loading (%

3.3.4 Cr(VI) Removal Performance

The permeate of a 5 mg/L Cr(VI) solution was collected using crossflow filtration at constant 2 bar pressure and submitted to AAS. Figure 16 shows that the adsorption Cr(VI) removal demonstrated to improve with increased PCB450 loading (wt.%). This correlates to all the previous analysis of higher porosity and hydrophilicity achieved at PCB loading 0.5 wt.% thus achieved highest Cr(VI) removal which is 33.33 %. Improvement of 30 % was recorded as opposed to pure membrane with 0 wt.% Further loading tested at 1 wt.% shows declined Cr(VI) removal of 15%. PCB450 loading. Although lower Cr(VI) removal recorded for MPCB 0.5 wt.% as compared to the PCB450 Cr(VI) removal through optimized revaluation adsorption tests at 27.98 %. Therefore, MPCB 0.5 wt.% shows significant improvement of Cr(VI) removal via membrane separation rather than a regular PCB450 batch adsorption test.

3.4 Future Works and Potential PCB450 Improvement as Adsorbent

Since PCB450 is optimized for Cr(VI) removal, future work should explore its use in membrane applications. The copra biochar formation shows potential with developed pores at an optimized pyrolysis temperature of 450 °C.

However, imperfections in the pores hinder Cr adsorption, likely due to volatile components interfering with carbonization. Torrefaction, as a heat pre-treatment, is recommended before pyrolysis at 450 °C to focus on volatilization and improve pore formation [40]. Additionally, chemical activation could enhance Cr(VI) adsorption and surface charge interactions. Combining physical and chemical modification will address the biochar's surface area limitation [41, 42].

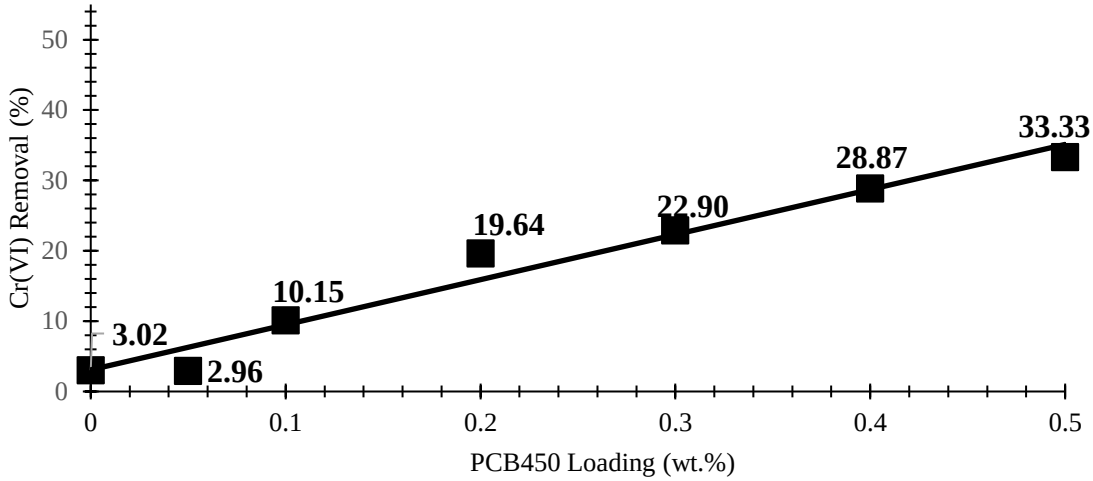

Figure 16 Cr(VI) removal against Weight Percentage of PCB450 Loading (%)

4.0 CONCLUSION

As the pyrolysis temperature increased from 300 °C to 550 °C, the percentage of copra biochar yield decreased (23.54 wt.% to 13.97 wt.%) but recorded to increase in carbon density of the biochar (23.6 wt.% to 16.3 wt.%) promoted dehydration, volatilization and carbonization which encouraged hydrogen and oxygen removal thus decreasing H/C and O/C Ratio. These results further concurred by declining presence of functional groups recorded through FTIR. This aligns with the increased pH_{pzc}, or basicity, of copra biochar, where biochar pyrolyzed below 500 °C is more acidic, and PCB550 exhibits the highest basicity. SEM and BET results both proved optimum pores formation occurs at 450 °C with pore sizes range (325-350) µm, highest total pore volume ($6.168x10^{-3}$ cm^3/g) with highest surface area achieved 1.865 m^2/g. Therefore, adsorption capacity and Cr(VI) removal increases with the highest record by the optimized 0.1 g/L PCB450, which acquired maximum value of 27.98 % Cr(VI) removal under optimized parameter of initial concentration 5 mg/L, pH 2 in 2 hours. Preliminary application of PCB450 incorporation in PVDF/PVP membrane improve water uptake and porosity optimized at 0.5 wt.% loading thus improve membrane water flux and Cr(VI) permeation achieved 33.33% removal.

ACKNOWLEDGEMENT

The authors gratefully acknowledge Universiti Teknologi Malaysia and the financial support from HICOE PY/2024/00042, R.J130000. 7801.4J664, the Ministry of Higher Education Malaysia under the Fundamental Research Grant Scheme, FRGS/1/2023/TK09/UTM/02/1,R.J130 000.7846.5F645, and UTM Fundamental Research PY/2024/00966, Q.J130000. 3846.24H14. The authors are appreciative for the opportunity and financial support provided by the Ministry of Higher Education (MOHE) and Universiti Teknologi Malaysia (UTM) to conduct this study. The authors would also like to thank the Research Management Centre (RMC) and Pusat Pengurusan Makmal Universiti (PPMU), Universiti Teknologi Malaysia for the technical support and services provided.

CONFLICTS OF INTEREST

The author(s) declare(s) that there is no conflict of interest regarding the publication of this paper.

REFERENCES

[1] Khandgave, S. S., Sreedhar, I. (2023). A mini review on engineered biochars as emerging adsorbents in heavy metal removal. *Mater Today Proc.*, 19–26.

[2] World Health Organization. (2022). Guidelines for drinking-water quality: Fourth edition incorporating the first and second addenda. World Health Organization, 1–614.

[3] Mitra, S., Chakraborty, A. J., Tareq, A. M., Emran, T. Bin, Nainu, F., Khusro, A., Idris, A. M., Khandaker, M. U., Osman, H., Alhumaydhi, F. A., Simal-Gandara, J. (2022). Impact of heavy metals on the environment and human health: Novel therapeutic insights to counter the toxicity. *J King Saud Univ Sci.*, *34*(3), 101865.

[4] Monga, A., Fulke, A. B., Dasgupta, D. (2022). Recent developments in essentiality of trivalent chromium and toxicity of hexavalent chromium: Implications on human health and remediation strategies. *Journal of Hazardous Materials Advances*, *7*, 100113.

[5] Chen, F., Guo, S., Wang, Y., Ma, L., Li, B., Song, Z., Huang, L., Zhang, W. (2022). Concurrent adsorption and reduction of chromium(VI) to chromium(III) using nitrogen-doped porous carbon adsorbent derived from loofah sponge. *Front Environ Sci Eng*. Doi: 10.1007/s11783-021-1491-6.

[6] Fourth edition incorporating the first and second addenda Guidelines for drinking-water quality.

[7] Oladimeji, T. E., Oyedemi, M., Emetere, M. E., Agboola, O., Adeoye, J. B., Odunlami, O. A. (2024). Review on the impact of heavy metals from industrial wastewater effluent and removal technologies. *Heliyon*, *10*(23), e40370.

[8] Liang, L., Xi, F., Tan, W., Meng, X., Hu, B., Wang, X. (2021). Review of organic and inorganic pollutants removal by biochar and biochar-based composites. *Biochar.*, *3*(3), 255–281.

[9] Sajjadi, B., Zubatiuk, T., Leszczynska, D., Leszczynski, J., Chen, W. Y. (2019). Chemical activation of biochar for energy and environmental applications: A comprehensive review. *Reviews in Chemical Engineering*, *35*(7), 777–815.

[10] Kumar Mishra, R., Singh, B., Acharya, B. (2024). A comprehensive review on activated carbon from pyrolysis of lignocellulosic biomass: An application for energy and the environment. *Carbon Resources Conversion*, *7*(4), 100228.

[11] Noor, N. M., Shariff, A., Abdullah, N., Syairah, N., Aziz, M. (2019). Temperature effect on biochar properties from slow pyrolysis of coconut flesh waste. *Malaysian Journal of Fundamental and Applied Sciences*, *15*(2), 153–158.

[12] Mohd H., Zakaria, M., Zaffrie, M., Amin, M., Faireal, A., Syafiq, M., Dani, A., Zakaria, M. H., Zaffrie, M., Amin, M., Ahmad, M. F. (2022). Market potential and competitiveness

assessment of Malaysian coconut-based products. *Econ Technol. Management Rev., 18*, 11–22.

[13] Wang, X., Zhao, Y., Tian, E., Li, J., Ren, Y. (2018). Graphene oxide-based polymeric membranes for water treatment. *Adv Mater Interfaces, 5*(15), 1701427.

[14] Infurna, G., Caruso, G., Dintcheva, N. T. (2023). Sustainable materials containing biochar particles: A review. *Polymers. 15*(2), 343.

[15] Lan, Y., Yan, N., Wang, W. (2018). Optimization of the PDMS/biochar nanocomposite membranes using the response surface methodology. *IEEE Journal of Selected Topics in Quantum Electronics, 25*(5), 947–956.

[16] Wang, K., Ye, Q., Shen, Y., Wang, Y., Hong, Q., Zhang, C., Liu, M., Wang, H. (2023). Biochar addition in membrane bioreactor enables membrane fouling alleviation and nitrogen removal improvement for low C/N municipal wastewater treatment. *Membranes (Basel), 13*(2), 194.

[17] Davenport, D. M., Gui, M., Ormsbee, L. R., Bhattacharyya, D. (2016). Development of PVDF membrane nanocomposites via various functionalization approaches for environmental applications. *Polymers*, *8*(2), 32.

[18] Kim, K., Young Ko, S., Park, J-O., - al, Alwin, S., Bhat, S. D., Sahu, A. K., Mhlanga, S. D., Tshabalala, T. G., Nxumalo, E. N., Mamba, B. B. (2014). Synthesis of PVDF ultrafiltration membranes supported on polyester fabrics for separation of organic matter from water. *IOP Conf Ser Mater Sci Eng., 64*(1), 012036.

[19] Janu, R., Mrlik, V., Ribitsch, D., Hofman, J., Sedláček, P., Bielská, L., Soja, G. (2021). Biochar surface functional groups as affected by biomass feedstock, biochar composition and pyrolysis temperature. *Carbon Resources Conversion, 4*, 36–46.

[20] Skic, K., Adamczuk, A., Gryta, A., Boguta, P., Tóth, T., Jozefaciuk, G. (2024). Surface areas and adsorption energies of biochars estimated from nitrogen and water vapour adsorption isotherms. *Scientific Reports, 14*(1), 1–14.

[21] Zhang, X., Zhao, B., Liu, H., Zhao, Y., Li, L. (2022). Effects of pyrolysis temperature on biochar's characteristics and speciation and environmental risks of heavy metals in sewage sludge biochars. *Environ Technol Innov., 26*, 102288.

[22] Yang, C., Liu, J., Lu, S. (2021). Pyrolysis temperature affects pore characteristics of rice straw and canola stalk biochars and biochar-amended soils. *Geoderma*. Doi: 10.1016/J.GEODERMA.2021.115097.

[23] Fan, L. Q., Liu, Wan, Y., Wang, Miao, J. X., Cai. J., Chen, W., Chen, F. H., Cheng, L., Ji, L., Luo, H. B. (2019). Hexavalent chromium adsorption removal from aqueous solution by fe-modified biochar derived from rice straw. *Appl Ecol Environ Res., 17*, 15311–15327. Doi: 10.15666/aeer/1706_153111532 7.

[24] Li, J., Jin, P., Tang, C. (2014). Cr(III) adsorption by fluorinated activated boron nitride: A combined experimental and

theoretical investigation. *RSC Adv.*, *4*(29), 14815–14821.

[25] Rajapaksha, A. U., Alam, M. S., Chen, N., Alessi, D. S., Igalavithana, A. D., Tsang, D. C. W., Ok, Y. S. (2018). Removal of hexavalent chromium in aqueous solutions using biochar: Chemical and spectroscopic investigations. *Science of the Total Environment*, *625*, 1567–1573.

[26] Huo, H., Hu, X., Wang, H., Li, J., Xie, G., Tan, X., Jin, Q., Zhou, D., Li, C., Qiu, G., Liu, Y. (2019). Synergy of photocatalysis and adsorption for simultaneous removal of hexavalent chromium and methylene blue by g-C_3N_4/$BiFeO_3$/carbon nanotubes ternary composites. *International Journal of Environmental Research and Public Health*, *16*(17), 3219.

[27] Shakya, A., Vithanage, M., Agarwal, T. (2022). Influence of pyrolysis temperature on biochar properties and Cr(VI) adsorption from water with groundnut shell biochars: Mechanistic approach. *Environ Res.*, *215*, 114243.

[28] Vo, A. T., Nguyen, V. P., Ouakouak, A., Nieva, A., Doma, B. T., Tran, H. N., Chao, H. P. (2019). Efficient removal of Cr(VI) from water by biochar and activated carbon prepared through hydrothermal carbonization and pyrolysis: adsorption-coupled reduction mechanism. *Water*, *11*(6), 1164.

[29] Yin, W., Guo, Z., Zhao, C., Xu, J. (2019). Removal of Cr(VI) from aqueous media by biochar derived from mixture biomass precursors of Acorus calamus Linn. and feather waste. *J Anal Appl Pyrolysis*, *140*, 86–92.

[30] Li, A., Deng, H., Jiang, Y., Ye, C. (2020). High-efficiency removal of Cr(VI) from wastewater by mg-loaded biochars: adsorption process and removal mechanism. *Materials*, *13*(4), 947.

[31] Xu, M., Wu, J., Luo, L., Yang, G., Zhang, X., Peng, H., Yu, X., Wang, L. (2018). The factors affecting biochar application in restoring heavy metal-polluted soil and its potential applications. *Chemistry and Ecology*, *34*(2), 177–197.

[32] Liu, L., Deng, G., Shi, X. (2020). Adsorption characteristics and mechanism of p-nitrophenol by pine sawdust biochar samples produced at different pyrolysis temperatures. *Scientific Reports*, *10*(1), 1–11.

[33] Vo, A. T., Nguyen, V. P., Ouakouak, A., Nieva, A., Doma, B. T., Tran, H. N., Chao, H. P. (2019). Efficient removal of Cr(VI) from water by biochar and activated carbon prepared through hydrothermal carbonization and pyrolysis: adsorption-coupled reduction mechanism. *Water*, *11*(6), 1164.

[34] Xu, M., Wu, J., Luo, L., Yang, G., Zhang, X., Peng, H., Yu, X., Wang, L. (2018). The factors affecting biochar application in restoring heavy metal-polluted soil and its potential applications. *Chemistry and Ecology*, *34*(2), 177–197.

[35] Tang, J. X., Jin, Y. T., He, Z. L., Hou, Q. Y., Zhao, C. T. (2018). A review of researches on biochar adsorbing organic contaminants and its mechanism and influence factors. *IOP Conf Ser Mater Sci Eng.*, *392*(5), 052030.

[36] Ezugbe, E. O., Rathilal, S. (2020). Membrane technologies

in wastewater treatment: a review. *Membranes (Basel), 10*(5), 89.

[37] Aziz, S., Mazhar, A. R., Ubaid, A., Shah, S. M. H., Riaz, Y., Talha, T., Jung, D. W. (2024). A comprehensive review of membrane-based water filtration techniques. *Appl Water Sci., 14*(8), 1–17.

[38] Miao, A., Wei, M., Xu, F., Wang, Y. (2020). Influence of membrane hydrophilicity on water permeability: An experimental study bridging simulations. *J Memb Sci., 604*, 118087.

[39] Hebbar, R. S., Isloor, A. M., Ismail, A. F. (2017). Contact angle measurements. *Membrane Characterization*, 219–255.

[40] Liang, M., Ding, Y., Zhang, Q., Wang, D., Li, H., Lu, L. (2020). Removal of aqueous Cr(VI) by magnetic biochar derived from bagasse. *Scientific Reports*, *10*(1), 1–13.

[41] Wang, P., Su, Y., Xie, Y., Zhang, S., Xiong, Y. (2019). Influence of torrefaction on properties of activated carbon obtained from physical activation of pyrolysis char. *Energy Sources, Part A: Recovery, Utilization, and Environmental Effects, 41*(18), 2246–2256.

[42] Janu, R., Mrlik, V., Ribitsch, D., Hofman, J., Sedláček, P., Bielská, L., Soja, G. (2021). Biochar surface functional groups as affected by biomass feedstock, biochar composition and pyrolysis temperature. *Carbon Resources Conversion*, *4*, 36–46.

[43] Sahu, N., Shukla, S., Chaudhary, V. K., Kumar, S. (2024). Effective Cr(Vi) removal from aqueous solution by novel biochar based-iron-oxide composites derived from chemical-carbonization of agricultural-waste: performance, kinetics, and mechanisms. Doi: 10.2139/SSRN.4965498.

[44] Ali, A., Alharthi, S., Al-Shaalan, N. H., Naz, A., Fan, H. J. S. (2023). Efficient removal of hexavalent chromium (Cr(VI)) from wastewater using amide-modified biochar. *Molecules, 28*(13), 5146.

[45] Yang, W., Lei, G., Quan, S., Zhang, L., Wang, B., Hu, H., Li, L., Ma, H., Yin, C., Feng. F., Jing, Y. (2022). The removal of Cr(VI) from aqueous solutions with corn stalk biochar. *Int J Environ Res Public Health, 19*(21), 14188.

[46] Mohadi, R., Palapa, N. R., Taher, T., Siregar, P. M. S. B. N., Normah, Juleanti, N., Wijaya, A., Lesbani, A. (2021). Removal of Cr(VI) from aqueous solution by biochar derived from rice husk. *Communications in Science and Technology, 6*(1), 11–17.

[47] Ghorbani-Khosrowshahi, S., Behnajady, M. A. (2016). Chromium(VI) adsorption from aqueous solution by prepared biochar from Onopordom Heteracanthom. *International Journal of Environmental Science and Technology, 13*(7), 1803–1814.

[48] Khan, A. A., Naqvi, S. R., Ali, I., Arshad, M., AlMohamadi, H., Sikandar, U. (2023). Algal-derived biochar as an efficient adsorbent for removal of Cr (VI) in textile industry wastewater: Non-linear isotherm, kinetics and ANN studies. *Chemosphere, 316*, 137826.

[49] Acharya, C., Mohapatra, R. K., Sasmal, A., Panda, C. R., Thatoi, H. (2024). Effective remediation

of Cr(VI) using coconut coir-derived porous biochar: application of kinetics and isotherm approaches. *International Journal of Environmental Science and Technology*, *21*(10), 7249–7268.

[50] Jha, S., Gaur, R., Shahabuddin, S., Ahmad, I., Sridewi, N. (2022). Kinetic and isothermal investigations on the use of low cost coconut fiber-polyaniline composites for the removal of chromium from wastewater. *Polymers (Basel)*, *14*(20), 4264.

[51] Lee, T. Z. E., Sim, S. F. (2019). Application of coconut copra as biosorbent for removal of heavy metals. *Key Eng Mater.*, *797*, 3–12.